Metavalent bonding induced abnormal phonon transport in diamondlike structures: Beyond conventional theory

Loay Elalfy [1], Denis Music [2], and Ming Hu [3,*]

[1] *Materials Chemistry, RWTH Aachen University, 52074 Aachen, Germany*

[2] *Department of Materials Science and Applied Mathematics, Malmö University, SE-205 06 Malmö, Sweden*

[3] *Department of Mechanical Engineering, University of South Carolina, Columbia, South Carolina 29208, USA*

(Received 23 June 2020; revised 27 November 2020; accepted 8 February 2021; published 19 February 2021)

A phenomenon appears in a few examples of the chalcopyrites (space group *I*-42 *d*) where heavier atoms do not necessarily lead to lower lattice thermal conductivity, in contradiction with Keyes expression that formulates an inverse relation of thermal conductivity with mean atomic mass. Herewith, the thermal conductivity of $CuInSe_2$, $CuInTe_2$, $AgInSe_2$, and $AgInTe_2$ was calculated and compared at room temperature from the linearized Boltzmann transport equation using *ab initio* density functional theory. $CuInSe_2$ and $AgInSe_2$ solids exhibit lower lattice thermal conductivity than that of $CuInTe_2$ and $AgInTe_2$, respectively, despite the fact that Te atoms are significantly heavier than Se. A comparison between dispersion relation, the Grüneisen parameter, and projected density of states leads to the conclusion that anharmonic transverse acoustic modes in the form of anomalous vibrations of Cu and Ag cause the lower values of the thermal conductivity. By analyzing the electronic structure, the compounds under study fit perfectly into a recently defined region of the metavalent bonding well known for its pronounced anharmonicity. The insight gained from the current results deepens our understanding of the unusual heat transfer phenomenon related to the metavalent bonding and sheds light on design and discovery of thermally functional materials that break the prediction by the conventional theory.

DOI: 10.1103/PhysRevB.103.075203

Much effort has been directed towards tailoring thermal conductivity. On the one hand, some applications require very low thermal conductivity to facilitate generation or conservation of energy, such as thermoelectrics where a low thermal conductivity and high electrical conductivity is the key to achieve high efficiency conversion [1,2]. On the other hand, a high thermal conduction is desirable for heat dissipation in nanoelectronics or photovoltaics [3–5]. However, the dependence of thermal transport on the chemical and physical properties of a compound is complex and interdependent, which makes formulating a standard model to describe all correlations quite challenging. During the last decade or earlier, several studies probed the dependence of phonon anharmonicity on the electronic configuration, orbitals, and boding of different compounds, none of which provided explicit equations [6–16]. According to the Keyes expression, it is known for example that there is an inverse relation between the atomic masses or mean atomic weight of a compound and its thermal conductivity [17]. One common example includes group IV elements exhibiting the diamond structure (*Fd*-3 *m*), where the lightest diamond has the highest thermal conductivity of 2200 $W\,m^{-1}\,K^{-1}$, silicon being 156 $W\,m^{-1}\,K^{-1}$, and the heaviest germanium reaches the minimum of only 60 $W\,m^{-1}\,K^{-1}$ [18]. Such a trend still holds in diamondlike structures such as binary $A^{II}-B^{VI}$, $A^{III}-B^{V}$, and $A^{III}-B^{VI}$, as well as in ternary $A^{II}B^{III}C_2{}^{V}$ and $A^{I}B^{III}C_2{}^{VI}$ known as chalcopyrites (*I*-42 *d*) [18–20]. However, not all ternary chalcopyrites adhere to this rule. For example, $CuAlSe_2$ and $CuAlTe_2$ exhibit higher thermal conductivities than the lighter $CuAlS_2$ [20]. The same exception holds for $CuInTe_2$ vs $CuInSe_2$ and $AgInTe_2$ vs $AgInSe_2$ [20]. This behavior is not only limited to chalcopyrites but extends to other binary compounds including rare earth elements [11,21–25]. To date, this unusual behavior that heavier compounds possess higher thermal conductivity is still not well understood, even though these solids are isostructural and experimentally synthesized.

These unusual ternary compounds belong to $A^{I}B^{III}C_2{}^{VI}$ chalcopyrites, a group of compounds with electronic band gap in the range between 0.2 and 1.0 eV [20,26–30]. Such electronic properties have drawn extensive attention during the last decade for their applications in thermoelectrics and photovoltaics and water splitting [31–36]. In a previous study, those compounds were found to exhibit negative pressure dependence that was related to negative thermal expansion due to the rotatory vibrations caused by bond bending in a form of a guitar string that formulates the acoustic phonon modes [37]. However, no study has been performed on cross-comparing these materials with same structure but different mass.

In this study, the behavior of low thermal conductivity for lighter compounds rather than the heavier ones is explored from vibrational and electronic structure points of view. The study covers four different In-based chalcopyrites, namely, $CuInSe_2$, $CuInTe_2$, $AgInSe_2$, and $AgInTe_2$. This range of compounds is chosen to systematically explore their chemical properties and its effect on their anomalous transport properties.

*Author to whom correspondence should be addressed: hu@sc.edu

First principles based total energies were calculated in the framework of density functional theory (DFT) using the Vienna *ab initio* simulation package (VASP) [38–41] with a Monkhorst-Pack *k*-point grid of 6×6×6 and convergence condition of 10^{-8} eV. The chalcopyrite supercells were relaxed until a convergence condition of the interatomic forces was reached at 10^{-4} eV Å^{-1}. The exchange-correlation functional was modeled using the Perdew-Burke-Ernzerhof (PBE) [42,43] of the generalized gradient approximation (GGA). The modeling of the electronic wave functions utilized the projector augmented wave method (PAW) [44,45] with an energy cutoff of 800 eV. All calculations were performed on a 2×2×1 supercell of the conventional unit cell (64 atoms in total) that is theoretically big enough to capture up to the fifth nearest neighbor interactions. A conversion test was conducted on two supercell sizes of $AgInSe_2$. The thermal conductivity was calculated with a 3×3×1 supercell (144 atoms) to be 1.264 W m^{-1} K^{-1} which is only 0.001 W m^{-1} K^{-1} higher than that for the 2×2×1 supercell (64 atoms). Since the thermal transport in semiconductors is dominated by phonon-phonon scattering [46], only lattice thermal conductivity was considered in this study. The harmonic (second order) interatomic force constants (IFCs) were calculated using the finite displacement method as implemented in PHONOPY [47], where the energy derivatives were calculated to acquire the dynamical matrices. By transforming the dynamical matrices in the reciprocal space, the phonon dispersion curves were obtained, from which phonon group velocities were extracted. To obtain the thermal transport properties (i.e., phonon relaxation time and lattice thermal conductivity), the linearized Boltzmann transport equation (BTE) was solved using the SHENGBTE [48] package iteratively utilizing the harmonic and anharmonic (third order) IFCs. To calculate the anharmonic IFCs, the fourth neighbor interactions were taken into consideration that captures the fundamental phonon scattering processes embedded in the used software. The values for thermal conductivity considering the second, third, and fourth neighbor interactions are 3.35, 3.25, and 2.87 W m^{-1} K^{-1}, respectively. A *q*-point grid of 10×10×10 was used to map the reciprocal space of phonons for calculating the lattice thermal conductivity, after conducting a test up to a 13×13×13 *q*-point grid where the difference in lattice thermal conductivity was 0.08 W m^{-1} K^{-1} higher for a 12×12×12*q*-point grid and 0.11 W m^{-1} K^{-1} higher for a 13×13×13 *q*-point grid.

Net atomic charges and overlap populations were calculated using the density derived electrostatic and chemical (DDEC6) method as implemented in CHARGEMOL [49–51]. In this work, the shared charge is presented as twice the DDEC6 overlap population as it is a count of the electron pairs shared. The transferred charge was calculated directly from the DDEC6 net atomic charges on each atom.

The calculated lattice parameters of $CuInSe_2$, $CuInTe_2$, $AgInSe_2$, and $AgInTe_2$ crystals are presented in Table I and compared with experimental measurements [52,53]. The lattice constants *a* are overestimated by up to 2%, however, the deviations of *c*/*a* from the ideal ratio of 2 is accurately captured. Such overestimation in comparison with the experimentally determined lattice constant is common for GGA in treating the exchange-correlation energy [54].

TABLE I. The calculated lattice parameters for $CuInSe_2$, $CuInTe_2$, $AgInSe_2$, and $AgInTe_2$ and comparison with experimental values.

	a (Å)		*c*/*a*	
	This work	Experiment	This work	Experiment
$CuInSe_2$	5.884	5.781 [53]	2.012	2.013 [53]
$CuInTe_2$	6.303	6.194 [53]	2.007	2.004 [53]
$AgInSe_2$	6.218	6.137 [52]	1.931	1.925 [52]
$AgInTe_2$	6.581	6.443 [52]	1.978	1.961 [52]

Having the structural features of explored chalcopyrites captured with acceptable precision, the lattice thermal conductivity is then explored. The two Cu-containing compounds, namely $CuInSe_2$ and $CuInTe_2$, have a measured thermal conductivity of 4.6 and 6.0 W m^{-1} K^{-1}, respectively [26,55], while for $AgInSe_2$ and $AgInTe_2$, the reported thermal conductivity is 1.0 and 1.9 W m^{-1} K^{-1}, respectively [30,56]. Our calculated thermal conductivity from *ab initio* BTE of $CuInSe_2$, $CuInTe_2$, $AgInSe_2$, and $AgInTe_2$ is 6.6, 7.5, 1.3, and 2.9 W m^{-1} K^{-1}, while the Keyes formula (solved with quantities listed in Table II) gives values of 2.8, 2.4, 3.9, and 1.1 W m^{-1} K^{-1}, respectively. In comparison with the experimental values, we first notice that there is an overestimation of up to 30% in the absolute value of lattice thermal conductivity, being a rather common deviation between theoretical modeling and experiments [57]. Such overestimation is most likely due to the lack of defects and grain boundaries in the ideal compounds treated in theoretical studies. These imperfections in turn lead to scattering processes that are not captured in the computational models. This overestimation is acceptable since the aim of this study is to investigate the intrinsic abnormal trends of the lattice thermal conductivities of the different compounds instead of the precise absolute values. The main features of those results are that the thermal conductivity of $CuInTe_2$ and $AgInTe_2$ is almost 1.2 and 2.3 times of that of $CuInSe_2$ and $AgInSe_2$, respectively, despite the Te atoms being much heavier than Se atoms. The thermal conductivity of the selected compounds from the Keyes formula appears to follow the before mentioned inverse relation with mean atomic mass. This indicates that our DFT calculation successfully reproduced the abnormal phenomenon appearing in the chalcopyrites, where heavier atoms do not necessarily lead to lower lattice thermal conductivity, and confirmed the behavior

TABLE II. The total Grüneisen parameter, melting point, density, and mean atomic mass of the unit cell for $CuInSe_2$, $CuInTe_2$, $AgInSe_2$, and $AgInTe_2$.

Compound	Grüneisen parameter	Melting temperature (K)	Density (kg m^{-3})	Atomic mass (amu)
$AgInSe_2$	0.97	5436	1327	84.03
$AgInTe_2$	0.95	5728	1387	108.38
$CuInSe_2$	0.52	5442	780	95.13
$CuInTe_2$	0.79	5629	692	119.48

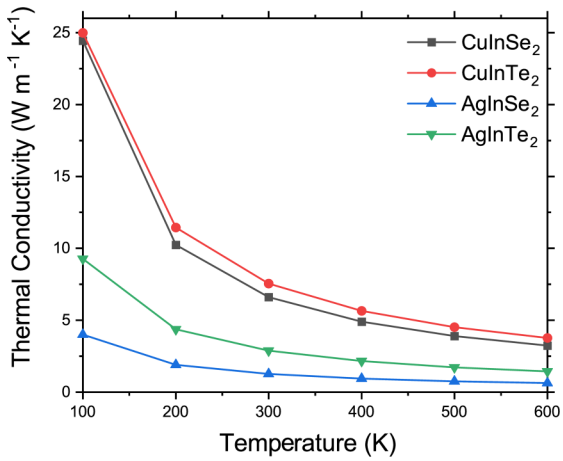

FIG. 1. Temperature dependent thermal conductivity of $CuInSe_2$, $CuInTe_2$, $AgInSe_2$, and $AgInTe_2$.

reported in previous experimental studies [20,26,56,58,59], while the Keyes formula failed to capture the correct behavior as it only includes the total Grüneisen parameter and does not account for the anharmonicity of the different modes. Figure 1 shows that the thermal conductivity is following the same trend for all compounds at different temperatures.

In order to understand the different contributions, with single relaxation time approximation the lattice thermal conductivity can be written as

$$\kappa = \sum_{\vec{q},p} C_V(\vec{q}, p)v^2(\vec{q}, p)\tau(\vec{q}, p),$$

where C_V is the mode dependent volume specific heat capacity, τ is the phonon relaxation time, and $\vec{q}$, p, are the wave vector and polarization of phonon modes, respectively. To understand the relation between lattice thermal conductivity and atomic masses, analysis of the different quantities contributing to the total thermal conductivity is essential. As for the constant volume specific heat capacity, the mode dependent quantities were calculated from the Einstein formula at 300 K and was found to have variation for different modes of less than 1% which agrees with the high temperature approximation for the Einstein solid. The total constant volume specific heat capacity was calculated to be 90.6, 91.2, 89.7, and 90.2 J mol^{-1} K^{-1} for $CuInSe_2$, $CuInTe_2$, $AgInSe_2$, and $AgInTe_2$, respectively, which is in good agreement with the available literature data [60]. Such minor heat capacity differences between these compounds in the range of 1% would not contribute to the thermal conductivity trends obtained herein.

The second and third factor to be analyzed is the phonon group velocity and relaxation time, which is harmonic and anharmonic properties reflected initially from the dispersion relation and the Grüneisen parameter [47,48], respectively. The interatomic force constants were calculated and in turn transformed to the frequency domains where the dynamical matrix was formulated to generate the phonon dispersion curves. Figure 2 shows the phonon dispersion for $CuInSe_2$, $CuInTe_2$, $AgInSe_2$, and $AgInTe_2$ along the high-symmetry path Γ-*X*-*P*-Γ in the first Brillouin zone, where the phonon mode dependent Grüneisen parameter (from negative to positive) is also indicated.

For all compounds, the vibrational frequency scales inversely with atomic masses, which is quite normal. At the *X*(0.5, 0, 0) point, the phonon frequencies of the transverse

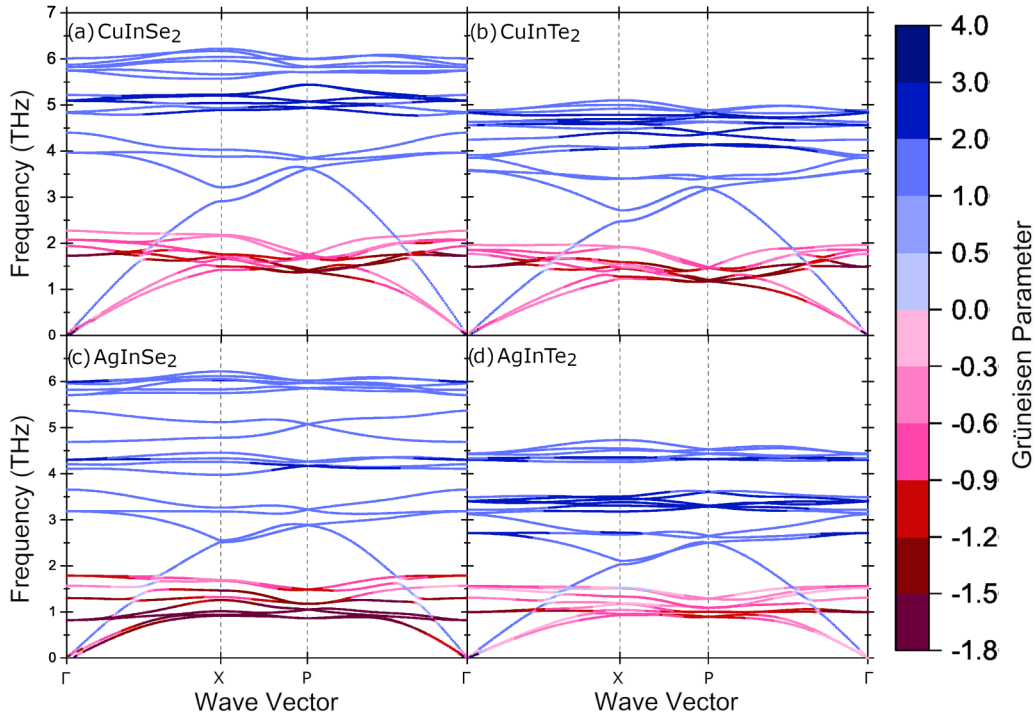

FIG. 2. Phonon dispersion relation and Grüneisen parameter of (a) $CuInSe_2$, (b) $CuInTe_2$, (c) $AgInSe_2$, and (d) $AgInTe_2$. The different color in the phonon dispersion indicates different Grüneisen parameter (from negative to positive) as indicated by the bar code.

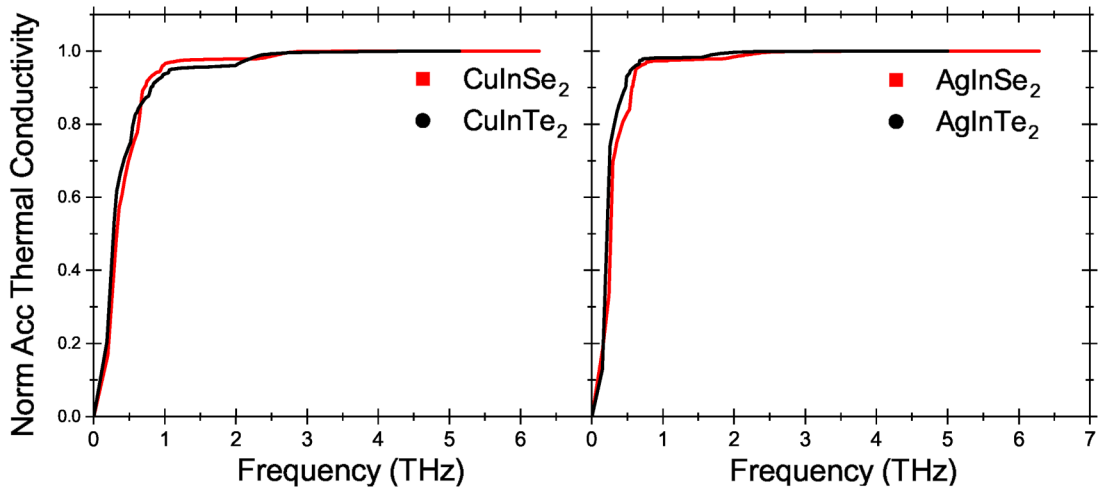

FIG. 3. Comparison of frequency dependent normalized accumlative thermal conductivity for $CuInSe_2$ and $CuInTe_2$ (left) and $AgInSe_2$ and $AgInTe_2$ (right).

acoustic (TA) modes occur at 1.49, 1.27, 0.94, and 0.96 THz for $CuInSe_2$, $CuInTe_2$, $AgInSe_2$, and $AgInTe_2$, respectively. Replacing Cu with Ag in a compound leads to a significantly lower frequency. This behavior is expected due to the higher mean atomic mass of Ag-containing materials than Cu-containing ones [61]. The same behavior occurs for replacing Se with Te in $CuInSe_2$. However, replacing lighter Se with heavier Te in $AgInSe_2$ leads to an opposite trend, which is in agreement with the literature [52], but not yet understood.

It is worth noticing that the acoustic (in particular TA) and some low optical phonon modes possess a negative Grüneisen parameter. The values of the Grüneisen parameter change for different compounds in a different fashion. For the TA modes at the *X* point, in the case of $CuInSe_2$ and $CuInTe_2$, the negative values increase from -1.5 to -1.0. As for $AgInSe_2$ and $AgInTe_2$, the Grüneisen parameter has values of -1.8 and -1.2, respectively. The negative Grüneisen parameter of the TA modes of chalcopyrites is well documented [62,63]. A higher magnitude of the Grüneisen parameter clearly implies a decrease in the lattice thermal conductivity, as there is an inverse square relation between the phonon relaxation time and the Grüneisen parameter according to the Debye-Callaway model [64]. As we can see below, the low frequency modes dominate the thermal conduction, and due to the higher anharmonicity of the TA modes in the selenides, the thermal conductivity of selenides tends to have lower values.

To quantify the importance of the low frequency modes, the accumulative thermal conductivity with respect to frequency is plotted in Fig. 3. For all compounds, a cutoff of the values for the TA modes constitutes up to 97% of the thermal conductivity, which indicates that the low frequency acoustic modes are almost entirely responsible for the thermal conductivity behavior and are the dominant heat carriers in all compounds explored in this work. In Fig. 4 the phonon group velocity is compared for each pair of compounds. For a cutoff of the value for the TA modes, the phonon group velocity is lower for the tellurides than that for the selenides. This is actually a factor contributing to a higher thermal conductivity of the selenides, which indicates that the low thermal conductivity of the selenides found in the DFT calculation should be *solely* due to the phonon anharmonicity (i.e., low phonon relaxation time). This is consistent with the discussion of the Grüneisen parameter trends indicating that the selenides are more anharmonic. In Fig. 5 the weighted phase space of phonon scattering is plotted, where it shows that the phase space for the tellurides is larger than that for the selenides, which shows that the harmonic phonon properties are not contributing to the reported trend. In Fig. 6 the phonon lifetime is plotted for different phonon modes. For the Cu-based systems with TA cutoff of up to 1.49 THz, the phonon lifetime of $CuInSe_2$ close to the Γ point (low values of the Grüneisen parameter as shown in Fig. 2) is slightly higher. As the anharmonic behavior is more dominant at the boundary of the first Brillouin zone, the phonons of $CuInSe_2$ are characterized by a lower lifetime of up to half the value of those for $CuInTe_2$. In the case of the Ag-based compounds, the phonon lifetime of $AgInSe_2$ is lower than $AgInTe_2$ over all the frequency range up to the TA cutoff. Hence, the differences in heat capacity and phonon group velocity do not account for the obtained difference in the magnitude of the thermal conductivity. The striking difference in the phonon lifetime due to the higher anharmonicity of the selenides is the main factor leading to the low thermal conductivity.

To understand the origin of the anharmonicity increase in lighter compounds, the projected vibrational density of states (VDOS) was explored and is shown in Fig. 7. The VDOS of the acoustic and low optical phonon modes constitute the first band. In the TA modes, the dominating factor of the thermal conductivity appears as the first peak in all compounds. The first evident difference between the different compounds is the fact that the vibrational density of states of the TA modes for the Cu-based compounds [Figs. 7(a) and 7(b)] is lower than that for the Ag-based compounds [Figs. 7(c) and 7(d)], which is due to spreading the same TA states over a longer frequency range. Looking at the projections for the Cu-based compounds, the Cu atoms do not contribute significantly to the lattice vibrations. For $CuInSe_2$, the projections on In and Se atoms are equal and reach around 40%, leaving the remaining 20% of the VDOS to the Cu atoms, while for $CuInTe_2$ the Te atoms vibrations contribute more than 53% while the

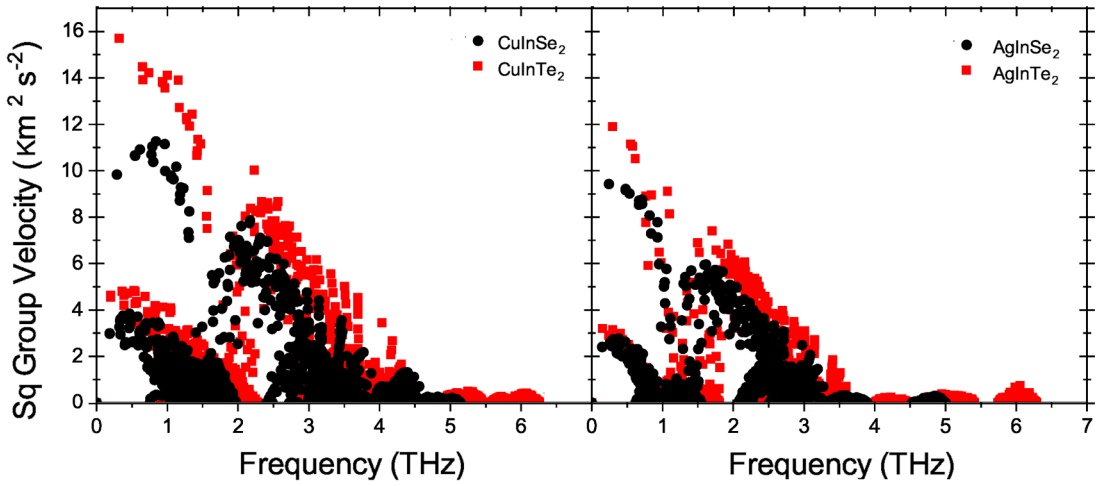

FIG. 4. Comparison of frequency dependent squared group velocity for $CuInSe_2$ and $CuInTe_2$ (left) and $AgInSe_2$ and $AgInTe_2$ (right). The tellurides generally have lower group velocities than selenides, which cannot explain the lower lattice thermal conductivity of selenides than tellurides.

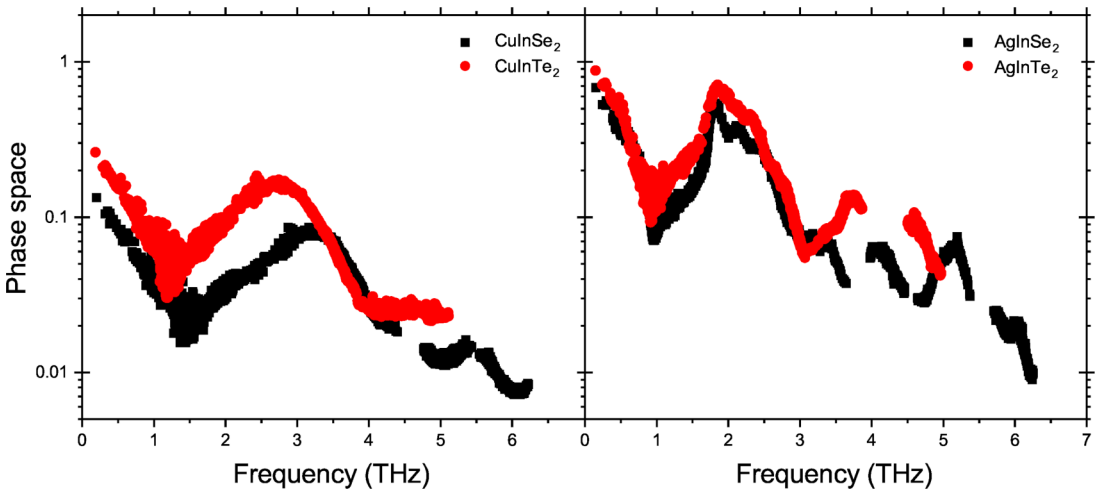

FIG. 5. Comparison of frequency dependent weighted phase space for $CuInSe_2$ and $CuInTe_2$ (left) and $AgInSe_2$ and $AgInTe_2$ (right). The tellurides generally have larger phase space than selenides, which cannot explain the stronger phonon anharmonicity of selenides than tellurides.

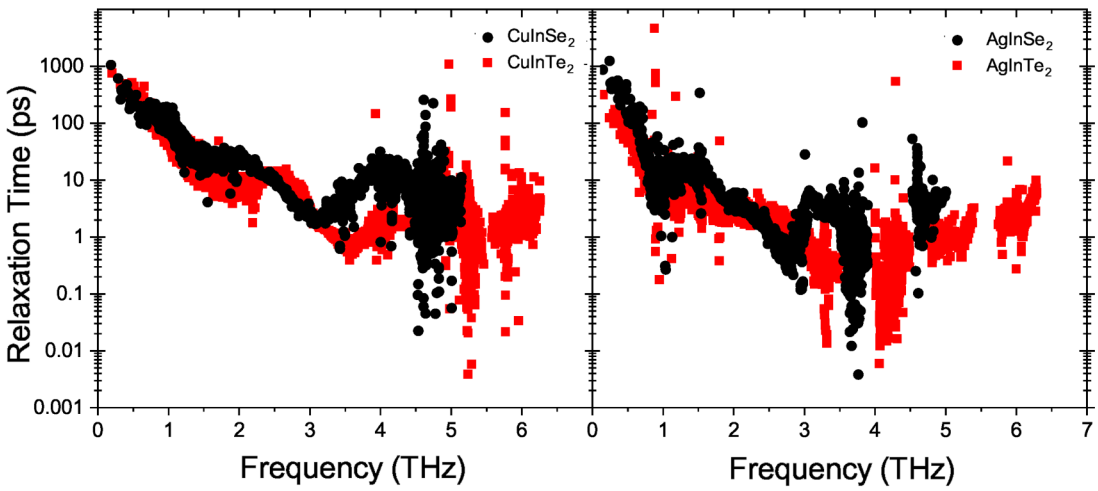

FIG. 6. Comparison of frequency dependent phonon relaxation time for $CuInSe_2$ and $CuInTe_2$ (left) and $AgInSe_2$ and $AgInTe_2$ (right).

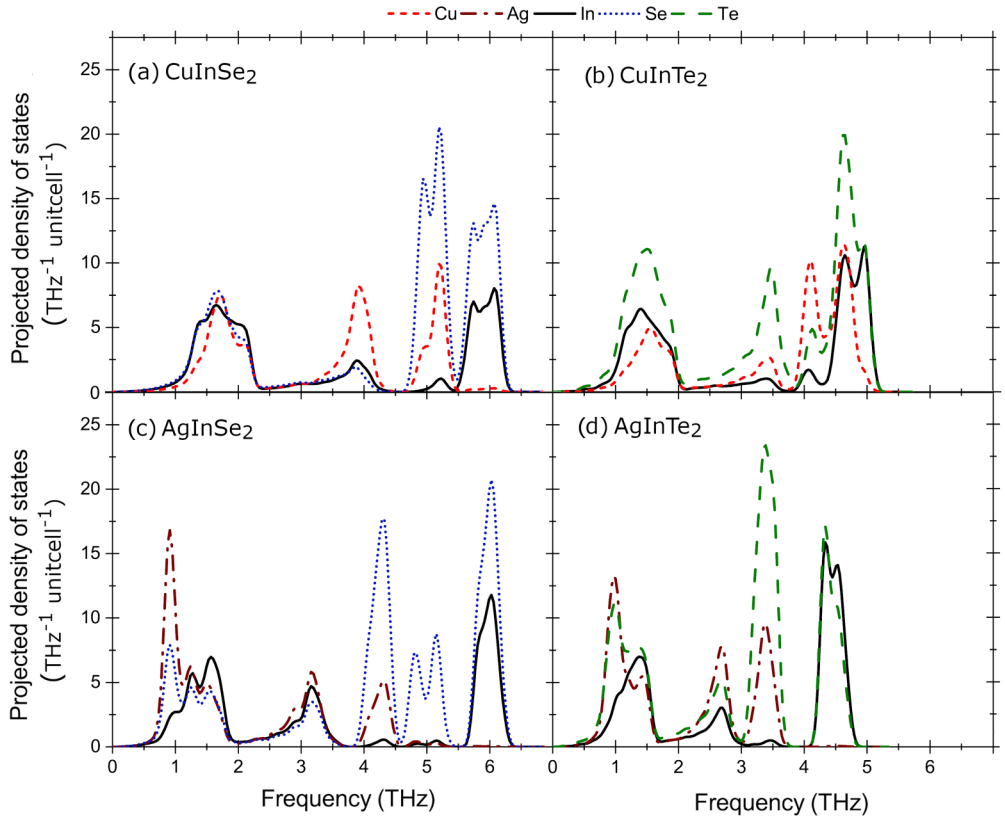

FIG. 7. Vibrational density of states for $CuInSe_2$, $CuInTe_2$, $AgInSe_2$, and $AgInTe_2$ projected on each atom.

contribution of In atoms is dropped to 33% and only 14% for the Cu atoms. As for Ag-based compounds, the TA modes are dominated by the vibrations of Ag and C^{VI} atoms in $A^{I}B^{III}C_2{}^{VI}$. The TA peak in $AgInSe_2$ constitutes 64% of the projection on Ag atoms and 30% on the Se atoms, while in $AgInTe_2$ Ag atoms contribute 53% and Te 41%. In both compounds, In atoms only contribute 6% to the VDOS of the TA modes. The analysis of the VDOS implies a different behavior for the Cu- and Ag-based compounds. The TA modes of the Cu-based compounds are dominated by the vibrations of In and C^{VI} atoms in $A^{I}B^{III}C_2{}^{VI}$, while in the Ag-based systems it is the vibration of Ag and C^{VI}. The common behavior is that the role of the Cu/Ag atoms decreases in tellurides in comparison with selenides, and that the contribution of the C^{VI} atoms in $A^{I}B^{III}C_2{}^{VI}$ barely changes in either compound. In this insight, a further analysis of the electronic structure is essential.

From a fundamental point of view, both compounds are isoelectronic (the same number of valence electrons), however, the atomic radii and electronegativity scales are different. To account for the effect of the electronegativity, the shared and transferred charge between each atom should be explored. Bonds are formed between A^{I} and C^{VI} as well as In and C^{VI} atoms (A^{I} = Cu and Ag, C^{VI} = Se and Te) in $A^{I}B^{III}C_2{}^{VI}$. Table III presents the amount of charge localized at each atom and shared between them. Regarding the ionicity of the constituting atoms, replacing Cu with Ag does not affect the charge transfer significantly, while selenides are more ionic than tellurides. When considering covalency, the Cu-C^{VI} bonds share more charge than Ag-C^{VI}, while the A^{I}-Se bonds share less charge than A^{I}-Te. On the other hand, In atoms share less charge with C^{VI} atoms in the Cu-based compounds in comparison with the Ag-based compounds. The difference in covalency between the Ag- and Cu-based compounds explains why the In contributes to the TA modes of the Cu-based systems.

To further quantify this behavior, the shared and transferred charges for the whole lattice was calculated so they could fit into a two-dimensional plot comparing the ionicity and covalency of the compounds. The shared charges for all compounds are similar at around $0.9|e|$, while the transferred charge in the selenides is around $0.55|e|$ and only $0.35|e|$ for the tellurides. This behavior of intermediate electron share and transfer was discussed very recently, where compounds were classified based on the type of bonding [15]. The main categories were naturally covalent, ionic, and metallic. However, a region between the conventional covalent and metallic

TABLE III. The transferred and shared charges between atoms in $CuInSe_2$, $CuInTe_2$, $AgInSe_2$, and $AgInTe_2$.

	Transferred charge ($\|e\|$)			Shared charge ($\|e\|$)	
	A^{I} (Cu or Ag)	In	C^{VI} (Se or Te)	A^{I}-C^{VI}	In-C^{VI}
$CuInSe_2$	0.328	0.738	−0.533	0.918	0.938
$CuInTe_2$	0.187	0.525	−0.355	0.96	0.948
$AgInSe_2$	0.319	0.772	−0.546	0.838	0.978
$AgInTe_2$	0.194	0.545	−0.370	0.906	0.972

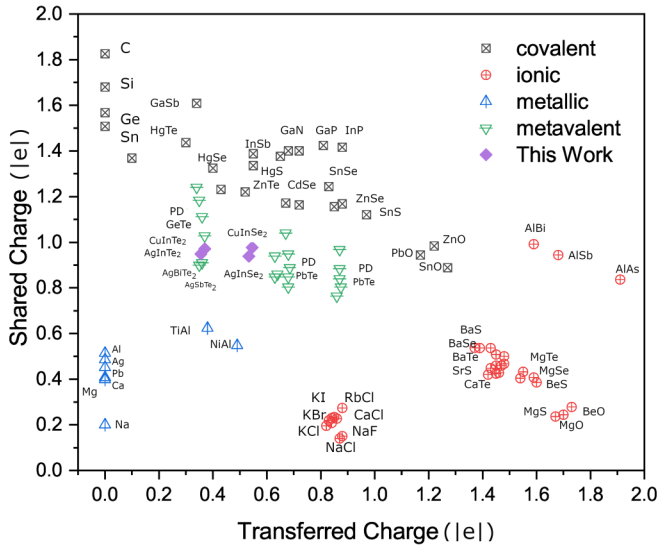

FIG. 8. Charge sharing vs charge transfer map where $CuInSe_2$, $CuInTe_2$, $AgInSe_2$, and $AgInTe_2$ studied herein belong to the metavalent bonding category, leading to strong intrinsic phonon anharmonicity. The data for materials other than $A^{I}InC_2{}^{VI}$ (A^{I} = Cu, Ag; C^{VI} = Se, Te) are taken from Ref [15]. Symbols labeled "PD" refer to the Peierls distorted structures of the same compound.

bonding was left with some compounds that did not belong to either group, as they share a unique bond breaking mechanism and large response properties [65,66]. Those compounds were characterized as a different class of bonding termed the metavalent bond. In fact, the compounds studied herein lie in the region of the newly defined metavalent bond as shown in Fig. 8 alongside other ternary chalcopyrites, such as PbTe. One of the relevant features of metavalent compounds is their strong anharmonicity, where the compounds with higher charge transfer are more anharmonic. The reason behind the compounds that are metavalently bonded is the deviation from the perfect tetrahedral structure. Due to the difference in atomic radii and electronegativity in ternary chalcopyrites, the bonds adopt angles deviating from regular 109 ° and the bond lengths are different. This provides the reason for the higher anharmonicity of the selenides than tellurides giving rise to lower thermal conductivity. The lower thermal conductivity of the lighter selenides than the tellurides due to the higher anharmonicity that was ascribed to the metavalent bonding provides guidance of how to select and tailor compounds with desired mechanical, electronic, and thermal properties.

In summary, the difference in atomic masses of isoelectronic and isostructural compounds usually contributes to a uniform change in thermal conductivity. However, there are several exceptions where lighter compounds tend to have lower thermal conductivity. This was studied through analyzing vibrational and thermal transport properties as well as identifying the physical origin. In the studied compounds $A^{I}InC_2{}^{VI}$ (A^{I} = Cu, Ag; C^{VI} = Te or Se), the lighter $CuInSe_2$ and $AgInSe_2$ possess unexpectedly lower thermal conductivity than the heavier $CuInTe_2$ and $AgInTe_2$, respectively. The transverse acoustic phonon bands, yielding the negative Grüneisen parameter, have a larger negative value for the selenides than tellurides. This is an indicator of stronger phonon anharmonicity and thus lower phonon lifetime, which is the main contribution to the low thermal conductivity. The Grüneisen theory proposes that a negative Grüneisen parameter is related to bonding mismatch, which is evidenced by the projected vibrational density of states. The low frequency phonons below the cutoff for transverse acoustic modes originate from the vibrations of In atoms in the Cu-based compounds and the Ag atoms in the Ag-based compounds. This may be understood based on the electronic structure. An average over the ionicity and covalency of different bonds ascribes the studied compounds to the metavalent bonding regime. The metavalent nature of the interatomic bonding rises from the distortion in the crystal lattice due to the variance in atomic radii and electronegativity, resulting in higher anharmonicity and finally lower lattice thermal conductivity of the selenides than tellurides. Our study pinpoints the root reason for the unusual heat transfer phenomenon related to the metavalent bonding in chalcopyrites, which is expected to impel further development and discovery of pertinent thermally functional materials that do not follow the trend predicted by conventional theory.

This work was supported by the Deutsche Forschungsgemeinschaft (DFG) within Project No. HU 2269/10-1. Simulations were performed with computing resources granted by JARA-HPC from RWTH Aachen University under Project No. JARA0131. Research reported in this publication was supported in part by the National Science Foundation (Award No. 2030128) and SC EPSCoR/IDeA Program under NSF OIA-1655740 via SC EPSCoR/IDeA 20-SA05.

[1] M. K. Jana and K. Biswas, ACS Energy Lett. **3**, 1315 (2018).
[2] X. Zhang and L.-D. Zhao, J. Materiomics **1**, 92 (2015).
[3] A. Makki, S. Omer, and H. Sabir, Renew. Sustain. Energy Rev. **41**, 658 (2015).
[4] E. Cuce, T. Bali, and S. A. Sekucoglu, Int. J. Low-Carbon Technol. **6**, 299 (2011).
[5] M. J. Huang, P. C. Eames, B. Norton, and N. J. Hewitt, Sol. Energy Mater. Sol. Cells **95**, 1598 (2011).
[6] R. Al Rahal Al Orabi, E. Orisakwe, D. Wee, B. Fontaine, R. Gautier, J.-F. Halet, and M. Fornari, J. Mater. Chem. A **3**, 9945 (2015).
[7] Y. Cheng, S. Wahl, and M. Wuttig, Phys. Status Solidi (RRL) 2000482 (2020).
[8] M. Dutta, K. Pal, U. V. Waghmare, and K. Biswas, Chem. Sci. **10**, 4905 (2019).
[9] A. Greco, S. Koval, and R. Migoni, J. Phys.: Condens. Matter **4**, 5291 (1992).

[10] H. Karakachian and M. Kazan, J. Appl. Phys. **122**, 045103 (2017).
[11] S. Lee, K. Esfarjani, T. Luo, J. Zhou, Z. Tian, and G. Chen, Nat. Commun. **5**, 3525 (2014).
[12] C. W. Li, J. Hong, A. F. May, D. Bansal, S. Chi, T. Hong, G. Ehlers, and O. Delaire, Nat. Phys. **11**, 1063 (2015).
[13] M. D. Nielsen, V. Ozolins, and J. P. Heremans, Energy Environ. Sci. **6**, 570 (2013).
[14] G. Qin, X. Zhang, S.-Y. Yue, Z. Qin, H. Wang, Y. Han, and M. Hu, Phys. Rev. B **94**, 165445 (2016).
[15] J.-Y. Raty, M. Schumacher, P. Golub, V. L. Deringer, C. Gatti, and M. Wuttig, Adv. Mater. **31**, 1806280 (2019).
[16] H. J. Tao, K. M. Ho, and X. Y. Zhu, Phys. Rev. B **34**, 8394 (1986).
[17] R. W. Keyes, Phys. Rev. **115**, 564 (1959).
[18] S. Adachi, J. Appl. Phys. **102**, 063502 (2007).
[19] W. O. Nakwaski, J. Appl. Phys. **64**, 159 (1988).
[20] M. L. Valeri-Gil and C. Rincón, Mater. Lett. **17**, 59 (1993).
[21] A. Seko, A. Togo, H. Hayashi, K. Tsuda, L. Chaput, and I. Tanaka, Phys. Rev. Lett. **115**, 205901 (2015).
[22] C. Li and D. Broido, Phys. Rev. B **95**, 205203 (2017).
[23] S. Ju, T. Shiga, L. Feng, and J. Shiomi, Phys. Rev. B **97**, 184305 (2018).
[24] A. A. El-Sharkawy, A. M. Abou El-Azm, M. I. Kenawy, A. S. Hillal, and H. M. Abu-Basha, Int. J. Thermophys. **4**, 261 (1983).
[25] J. M. Skelton, S. C. Parker, A. Togo, I. Tanaka, and A. Walsh, Phys. Rev. B **89**, 205203 (2014).
[26] J. Yao, N. J. Takas, M. L. Schliefert, D. S. Paprocki, P. E. R. Blanchard, H. Gou, A. Mar, C. L. Exstrom, S. A. Darveau, P. F. P. Poudeu, and J. A. Aitken, Phys. Rev. B **84**, 075203 (2011).
[27] H.-J. Wu, S.-W. Chen, T. Ikeda, and G. J. Snyder, Acta Mater. **60**, 6144 (2012).
[28] S. M. Ismailov, Z. A. Isaev, S. M. Orakova, and K. S. Yakh'yaeva, High Temp. **57**, 832 (2019).
[29] P. Z. Ying, H. Zhou, Y. L. Gao, Y. Y. Li, Y. P. Li, X. L. Lian, and J. L. Cui, Key Eng. Mater. **519**, 188 (2012).
[30] Y. Aikebaier, K. Kurosaki, T. Sugahara, Y. Ohishi, H. Muta, and S. Yamanaka, Mater. Sci. Eng. B **177**, 999 (2012).
[31] R. Herberholz, V. Nadenau, U. Rühle, C. Köble, H. W. Schock, and B. Dimmler, Sol. Energy Mater. Sol. Cells **49**, 227 (1997).
[32] J. Kaneshiro, N. Gaillard, R. Rocheleau, and E. Miller, Sol. Energy Mater. Sol. Cells **94**, 12 (2010).
[33] J. Luo, S. D. Tilley, L. Steier, M. Schreier, M. T. Mayer, H. J. Fan, and M. Grätzel, Nano Lett. **15**, 1395 (2015).
[34] B. Marsen, S. Dorn, B. Cole, R. E. Rocheleau, and E. L. Miller, MRS Proc. **974**, 0974-CC09-05 (2006).
[35] J. M. Raulot, C. Domain, and J. F. Guillemoles, J. Phys. Chem. Solids **66**, 2019 (2005).
[36] M. J. Romero, H. Du, G. Teeter, Y. Yan, and M. M. Al-Jassim, Phys. Rev. B **84**, 165324 (2011).
[37] L. Elalfy, D. Music, and M. Hu, Materials **12**, 3491 (2019).
[38] G. Kresse and J. Hafner, Phys. Rev. B **49**, 14251 (1994).
[39] G. Kresse and J. Hafner, Phys. Rev. B **47**, 558 (1993).
[40] G. Kresse and J. Furthmüller, Phys. Rev. B **54**, 11169 (1996).
[41] G. Kresse and J. Furthmüller, Comput. Mater. Sci. **6**, 15 (1996).
[42] J. P. Perdew, K. Burke, and M. Ernzerhof, Phys. Rev. Lett. **78**, 1396 (1997).
[43] J. P. Perdew, K. Burke, and M. Ernzerhof, Phys. Rev. Lett. **77**, 3865 (1996).
[44] P. E. Blöchl, Phys. Rev. B **50**, 17953 (1994).
[45] G. Kresse and D. Joubert, Phys. Rev. B **59**, 1758 (1999).
[46] R. Peierls, Ann. Phys. (Leipzig, Ger.) **395**, 1055 (1929).
[47] A. Togo and I. Tanaka, Scr. Mater. **108**, 1 (2015).
[48] W. Li, J. Carrete, N. A. Katcho, and N. Mingo, Comput. Phys. Commun. **185**, 1747 (2014).
[49] T. A. Manz and N. G. Limas, RSC Adv. **6**, 47771 (2016).
[50] N. G. Limas and T. A. Manz, RSC Adv. **6**, 45727 (2016).
[51] T. A. Manz, RSC Adv. **7**, 45552 (2017).
[52] A. V. Kopytov and A. V. Kosobutsky, Phys. Solid State **51**, 2115 (2009).
[53] K. S. Knight, Mater. Res. Bull. **27**, 161 (1992).
[54] L. He, F. Liu, G. Hautier, M. J. T. Oliveira, M. A. L. Marques, F. D. Vila, J. J. Rehr, G. M. Rignanese, and A. Zhou, Phys. Rev. B **89**, 064305 (2014).
[55] R. Liu, L. Xi, H. Liu, X. Shi, W. Zhang, and L. Chen, Chem. Commun. **48**, 3818 (2012).
[56] P. Qiu *et al.*, Adv. Sci. **5**, 1700727 (2018).
[57] T. Ouyang and M. Hu, Phys. Rev. B **92**, 235204 (2015).
[58] D. Zou, S. Xie, Y. Liu, J. Lin, and J. Li, J. Alloys Compd. **570**, 150 (2013).
[59] S. N. Rashkeev and W. R. L. Lambrecht, Phys. Rev. B **63**, 165212 (2001).
[60] A. V. Kopytov and A. V. Kosobutsky, Phys. Solid State **52**, 1359 (2010).
[61] L.-F. Huang and Z. Zeng, J. Phys. Chem. C **119**, 18779 (2015).
[62] Y. Zhang, E. Skoug, J. Cain, V. Ozoliņš, D. Morelli, and C. Wolverton, Phys. Rev. B **85**, 054306 (2012).
[63] J. Yang, Q. Fan, Y. Yu, and W. Zhang, Materials (Basel) **11**, 2370 (2018).
[64] J. Callaway, Phys. Rev. **113**, 1046 (1959).
[65] M. Zhu, O. Cojocaru-Mirédin, A. M. Mio, J. Keutgen, M. Küpers, Y. Yu, J.-Y. Cho, R. Dronskowski, and M. Wuttig, Adv. Mater. **30**, 1706735 (2018).
[66] M. Wuttig, V. L. Deringer, X. Gonze, C. Bichara, and J.-Y. Raty, Adv. Mater. **30**, 1803777 (2018).